IEICE TRANS. COMMUN., VOL.E97–B, NO.7 JULY 2014

INVITED PAPER *Joint Special Section on Opto-electronics and Communications for Future Optical Network*

Software Defined Flexible Optical Access Networks Enabling Throughput Optimization and OFDM-Based Dynamic Service Provisioning for Future Mobile Backhaul

Akihiro TANAKA[†a)], ***Member and*** **Neda CVIJETIC**[†], ***Nonmember***

SUMMARY In this invited paper, software defined network (SDN)-based approaches for future cost-effective optical mobile backhaul (MBH) networks are discussed, focusing on key principles, throughput optimization and dynamic service provisioning as its use cases. We propose a novel physical-layer aware throughput optimization algorithm that confirms > 100 Mb/s end-to-end per-cell throughputs with ≥2.5 Gb/s optical links deployed at legacy cell sites. We also demonstrate the first optical line terminal (OLT)-side optical Nyquist filtering of legacy 10G on-off-keying (OOK) signals, enabling dynamic >10 Gb/s Orthogonal Frequency Domain Multiple Access (OFDMA) λ-overlays for MBH over passive optical network (PON) with 40-km transmission distances and 1:128 splitting ratios, without any ONU-side equipment upgrades. The software defined flexible optical access network architecture described in this paper is thus highly promising for future MBH networks.

key words: *software defined network (SDN), mobile backhaul (MBH), passive optical network (PON), orthogonal frequency division multiple access (OFDMA), Nyquist filtering*

1. Introduction

Continuing exponential growth of Internet traffic is not giving the slightest indication of stagnation, driven by the rapid spread of bandwidth-hungry services such as online video streaming, large-capacity file transfer etc. In access networks, mobile backhaul (MBH) networks with many cell sites have become a bottleneck to delivering sufficient capacity to the end users, such that highly cost effective solutions for MBH are urgently required. Passive optical networks (PONs) have been regarded as a promising candidate for this purpose, attracting much recent attention [1]–[4]. However, in addition to the requirement for the high-speed communication links, network operators are also facing additional challenges of effectively coping with dynamic and unpredictable changes in the traffic demand. Legacy PON techniques cannot completely satisfy these additional requirements; a new futuristic network management approach is thus strongly required.

Given this situation, we have proposed a flex-grid dynamic λ-flow overlay architecture for MBH over legacy PON leveraging software-defined network (SDN)-based centralized control, and demonstrated simultaneous transmission of 10 Gb/s On-Off-Keying (OOK) and >10 Gb/s/λ Orthogonal Frequency Division Multiple Access (OFDMA) signals without the use of optical filtering, amplification, or coherent detection at the cost-sensitive optical network unit (ONU) side [5]. By applying this new architecture, high-speed OFDMA signals can be dynamically overlaid onto existing PON without optical equipment upgrade of legacy ONUs. However, the transmission distance and passive split ratio in [5] were restricted to 20 km with 1:64 split due to severe interference between OFDMA and OOK signals.

In this invited paper, we elaborate on the software defined optical access network architecture for future MBH, by discussing a novel throughput optimization algorithm with a global knowledge of physical-layer MBH topology [6]. The algorithm is evaluated for a heterogeneous optical/wireless last-mile small cell backhaul network, confirming 4G long term evolution (LTE)-compatible per-cell end-to-end throughputs of 141.1 Mb/s with 2.5 Gb/s fiber links at legacy macro cell sites. The SDN-based approach is thus attractive for optical MBH planning/optimization. We also propose optical line terminal (OLT)-side optical Nyquist filtering of legacy 10G OOK signals for OFDMA/OOK interference reduction and for the first time experimentally demonstrate that it doubles both the reach and split ratio of dynamic >10 Gb/s OFDMA λ-overlays over PON, without any ONU-side optics upgrades [7]. We experimentally demonstrate simultaneous 40-km standard single mode fiber (SSMF) reach with 1:128 passive split transmission of >10 Gb/s/λ OFDMA and OOK with direct detection and no ONU-side optical filtering or amplification. The new approach is highly attractive for cost-efficient, high-speed dynamic λ-overlays in deployed PON.

In the following, we first review our SDN-based approach for MBH applications and explain the proposed throughput optimization algorithm in Sect. 2. In Sect. 3, we describe the experimental demonstration of our proposed optical Nyquist filtering technique for reach and split ratio increases through OFDMA/OOK interference management.

2. Software Defined Optical Access Network

2.1 SDN Principles for Flexible Optical Access Networks

The key idea behind the SDN approach is that the network should be directly controlled by the demands of the services/applications it is delivering, and that this control

Manuscript received November 8, 2013.
Manuscript revised February 28, 2014.

[†]The authors are with NEC Laboratories America, Princeton, NJ 08540, USA.
a) E-mail: a-tanaka@dh.jp.nec.com

DOI: 10.1587/transcom.E97.B.1244

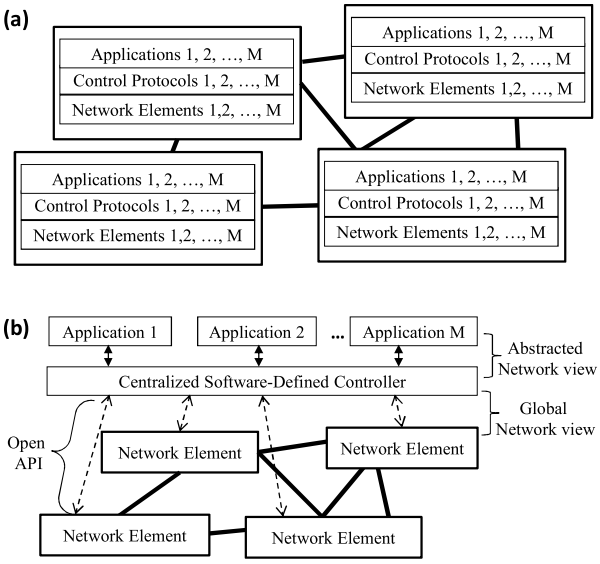

Fig. 1 Network control and data plane architecture for: (a) legacy distributed control; and (b) centralized SDN control [9].

should be easy and quick both to deploy, and to change [8], [9]. Consequently, in SDN, a centralized software-defined controller operating on top of general purpose hardware is envisioned (Fig. 1(b)), in place of distributed, protocol-specific controllers and customized hardware (Fig. 1(a)) that can increase network complexity and limit network reconfigurability [9]. A useful analogy can thus be drawn between the operation of a software defined network and a smart mobile device, for example. Just like the combination of applications running on a generic smart mobile device (e.g. phone, tablet, etc.) can be centrally controlled by the user on-demand through a software interface, so would the combination of services running on the same underlying network be centrally administered in software, enabling rapid and flexible network management, control and optimization.

Thus far, SDN has been successfully exploited in datacenter and smaller-scale networks which have generally have a high degree of network connectivity (e.g. fully-meshed topology) and a low degree of physical-layer constraints. Consequently, to effectively extend SDN principles to optical access networks, the dynamic resource management and virtualization principles of SDN need to be preserved, while taking into account the physical connectivity restrictions, legacy technology limitations, and fundamental fiber channel impairments that arise. Moreover, based on the analogy between a software-defined network and a smart phone, designing the right set of software-defined optical access network applications to support multiple broadband solutions is just as important in successfully relating underlying technology with revenue growth. Finally, given that costly fiber deployments for optical access are expected to remain largely unchanged in the foreseeable future, applying SDN principles to multi-service optical access should focus on the edge points of the network: namely, centralized control protocols at the OLT-side, reconfigurable network

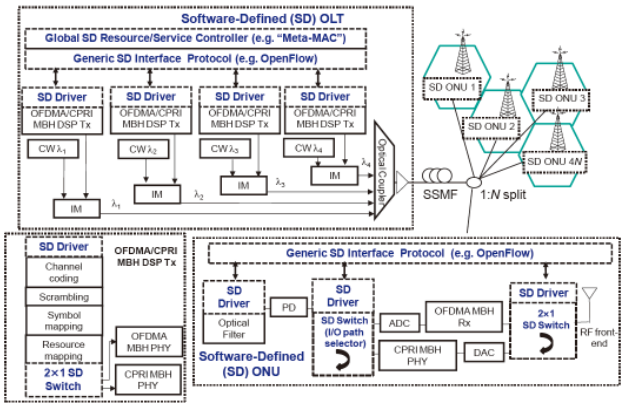

Fig. 2 Software-defined optical access architecture for multiple mobile backhaul (MBH) services [11].

applications for both the OLT and ONU sides, and highly efficient network resource optimization algorithms with a global view of the network topology. This will be discussed in detail in the following section through examples of each of the aforementioned topics.

2.2 Centralized Network Control for Future MBH

2.2.1 Software-defined Centralized Control via Meta-MAC

The point-to-multipoint passive optical network (PON) topology that is predominant in optical access networks already coincides with centralized network control architectures that are at the core of the SDN paradigm. In addition to efficiently centralizing the most computationally-demanding processing part, this approach also liberates the network from a priori service specificity. Namely, with software-based control and a global view of the network, the centralized controller can intelligently and rapidly size network resources to fit the incoming demands. As an example, Fig. 2 shows software-defined centralized resource/service control via the "meta-MAC" algorithm [10], which essentially abstracts physical-layer differences between services and exploits virtual sub-wavelength frequency domain slots/groups to delineate bandwidth pipes for each service. Essentially, the meta-MAC performs: 1) service admission and bandwidth assignment; and 2) spectrum allocation by periodically executing a resource optimization routine. Consequently, a trade-off emerges between frequent execution that increases computational complexity, increasing power consumption, and non-frequent execution that saves power but increases delay. Nonetheless, as shown in [10], with 8 simultaneous services, i.e. "virtual PONs" (VPONs), and 0.6 offered load, the total meta-MAC execution time was 70 ms, consuming just 7% of the overall bandwidth provisioning period, such that an energy-efficient sleep mode can be exploited during 93% of the provisioning cycle, while maintaining end-to-end delay <10 ms. Repeating the computation above for 14 VPONs, however, increased meta-MAC

execution time up to 400 ms, highlighting the trade-off between computational complexity and dynamic multi-service support in software-defined centralized control.

2.2.2 Software-defined "Apps": MBH Example

Since multiple MBH types may be needed in the future, a software reconfigurable solution that enables dual-mode common public radio interface (CPRI) vs. OFDMA MBH was introduced in [11]. As shown in Fig. 2, in this approach, depending on the MBH type, the software-defined driver of each OLT-side flexible transmitter selects the corresponding set of required functions; it is noted that, despite the differences between OFDMA and CPRI, overall functionality can feature a high degree of similarity (Fig. 2). At each MBH ONU, the service type assignments made by the centralized controller (e.g. meta-MAC) are communicated by the ONU-side interface protocol (e.g. OpenFlow) to configure optical and electronic hardware. As shown in [11], while fixed XG-PON MBH (static 10 Gb/s rate) could not adapt to real-time traffic, resulting in either bandwidth under or over provisioning, the software defined MBH approach closely followed the real-time traffic profile. Strong bit error rate (BER) performance was also confirmed using a $4\lambda \times 25.125$ Gb/s/λ = 100.5 Gb/s WDM-OFDMA-PON setup for up to 1024 ONUs [11]. Moreover, OFDMA-based λ overlay targeting MBH application, provisioning overlaid signals by the OpenFlow-based SDN controller over the legacy PON was demonstrated in [5]. By efficiently utilizing "unused" wavelengths in the legacy PONs' optical spectrum, 150 Mb/s per-cell OFDMA λoverlay for MBH with 64 ONUs was demonstrated, while minimizing negative impacts on the existing legacy services.

2.2.3 Software-defined Throughput Optimization for MBH

Once a centralized control protocol and flexible network platforms are provided, then innovative resource optimization algorithms are needed to enable efficient network management with respect to ceaselessly changing network traffic. As shown in Fig. 3, the proposed software defined algorithm [6] seeks to optimize throughput in an evolving MBH network composed of both legacy (macro) and emerging (small cell) sites. Specifically, given a MBH network of n nodes and global knowledge of physical-layer link parameters (Fig. 3(i)), is communicated via generic protocols (e.g. OpenFlow, Fig. 3(iii)), and the SD algorithm computes the maximum achievable throughput rate, r_{max}, between all $n/2$ communication pairs (Fig. 3(ii)), where the same r_{max} is required for all pairs for fairness. (Based on r_{max}, the aggregate network throughput can readily be computed as $r_{max} \times n/2$.) As shown in Fig. 3(i), (ii), (iv), the optimal value of r_{max} will depend on both the physical per-link rates in the network, as well as on optimized scheduling/routing of the MBH data flows. To translate both parameters into the throughput optimization problem, we define a set of rate

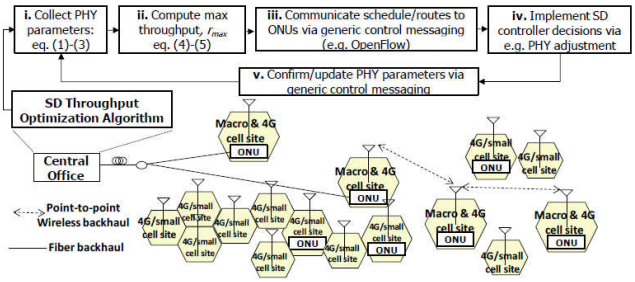

Fig. 3 SD throughput optimization architecture for optical MBH [6].

matrices, R, for the n-node network, wherein each R is a $n \times n$ matrix populated by physical per-link data rates, r_{ij}, such that: $r_{ij} = r_{ij}$ if node j receives information at rate r_{ij} from node i; $r_{ij} = -r_{ij}$ if j transmits information at rate r_{ij} from i; and $r_{ij} = 0$ otherwise. At any given time, $T = t$, the corresponding rate matrix, $R(t)$, thus contains all data flow information in the network. The rate matrix entries, r_{ij}, can then be computed based on the effective signal-to-noise ratio (SNR), ξ_{ij}, on each MBH link. For ideal additive white Gaussian noise (AWGN) channels, $r_{ij} = W_{ij} \log_2(1 + \xi_{ij})$, where ξ_{ij} is link SNR and W_{ij} is physical bandwidth. For non-ideal wireless MBH links, ξ_{ij} can be computed as

$$\xi_{ij} = \frac{G_{ij}P_i}{\sigma_j^2 + \sum_k G_{kj}P_k}, \tag{1}$$

where P_i is the transmitted power, G_{ij} is the channel gain coefficient, σ_j^2 is the AWGN noise variance, and the second term in the denominator accounts for any interference that is also treated as noise [12]. For point-to-point wireless links, ξ_{ij} may be computed as

$$\xi_{ij} = G_{ij}\frac{P_i}{\sigma_j^2}\frac{(2\pi)^2}{\theta_{ij}\theta_{ji}}\left(\frac{d_0}{d_{ij}}\right)^{\alpha}, \tag{2}$$

where θ_{ij} and θ_{ji} are the one-dimensional antenna beam widths, d_{ij} is the Euclidean distance between nodes i and j, and d_0 is the reference distance based on which the effect of the free-space path loss parameter α is computed [12]. Finally, for r_{ij} computation on optical fiber links, the SNR and optical SNR (OSNR) may be related as

$$OSNR_{ij} = \frac{\rho R_s}{2B_{ref}}\xi_{ij}, \tag{3}$$

where $\rho = 1, 2$ for single- and dual- polarization signals, respectively, R_s is the symbol rate, and B_{ref} is the OSNR reference bandwidth. To account for MBH traffic variability over time, T, and dynamically optimize scheduling/routing, the temporal evolution is modeled by fractional time slots $t_k \geq 0$, $\sum t_k = 1$, where N denotes the number of slots. The rate matrix of the dynamic network, R_{DN}, is then given by

$$R_{DN} = \sum_{k=1}^{N} t_k R_k, \tag{4}$$

wherein each R_k in (4) is populated by physical per-link rates

r_{ij} of (1)–(3). The optimal R_{DN} is then found by computing the schedule, $\{t_k,\ k = 1, \ldots, N\}$, which enables the highest effective throughput rate, r_{max}, between all communication pairs in the network. Mathematically, for a n-node network, the dimensionality of R_{DN} in (4) is isomorphic to vectors with length $n(n-1)$, such that (4) may be solved as a linear optimization problem in $N-1$ Euclidean space as

$$\begin{aligned} &\text{minimize } \sum_{k=1}^{N} t_k \\ &\text{subject to } R_{DN} = \sum_{k=1}^{N} t_k R_k \end{aligned} . \tag{5}$$

The result of (5) can then be exploited by the SD MBH controller (Fig. 3) to make the traffic routing/scheduling decisions that maximize overall throughput, as well as to identify network bottlenecks (i.e. those links/hops that require longer scheduling slots, t_k), and evaluate throughput effects of cell site MBH upgrades to fiber connectivity. Moreover, such optimization can be done in a software-reconfigurable way, accounting for real-time changes in traffic demands and patterns.

The proposed SD throughput maximization algorithm was evaluated on the MBH network of Fig. 4(a), formed by $n = 20$ nodes randomly distributed on a $3.75\,\text{km}^2 \approx 1.5\,\text{mi}^2$ (e.g. last mile) rectangular area and mapped into $n/2 = 10$ source-destination pairs. As shown in Fig. 4(a), each dark square denotes a new small cell ("pre-aggregation") site targeted for point-to-point wireless backhaul, while each light circle indicates a co-located legacy macro/new small-cell ("aggregation") site, already featuring legacy point-to-point wireless backhaul and potentially requiring an upgrade to fiber connectivity.

In other words, for the legacy MBH sites, which both originate traffic and must route traffic to/from other cells, the SD algorithm seeks to evaluate throughput effects of MBH link upgrades to optical fiber. To compute r_{max} for each target MBH case I-VI in Fig. 4(b), all per-link rates, r_{ij}, for the network in Fig. 4(a) were first calculated for the according to (1)–(3), wherein, unless otherwise noted $P_i = 0.1$ Watts, d_{ij} values were taken from the geometry of Fig. 4(a), d_0=70 m, $\alpha = 3$, $\sigma_j^2 = W_{ij} \times 10^{-5}$, $\rho = 1$, and $B_{ref} = 12.5$ GHz. A linear optimization routine was implemented in MATLAB to compute r_{max} using the rate matrix formulation of (4), (5), with the per-cell maximum throughput, r_{max}, plotted in Fig. 4(b) versus wireless MBH bandwidth, W_{ij} MHz; as shown in Fig. 4(b), for all cases, low W_{ij} values created severe local MBH bottlenecks and limited $r_{max} \leq 20$ Mb/s despite fiber connectivity, highlighting the importance of this parameter. As also shown in Fig. 4(b), while the upgrade of legacy sites to 1 Gb/s fiber backhaul (Case III) improved r_{max} compared to both all-wireless MBH scenarios (Cases I and II), an additional upgrade of legacy sites to 2.5 Gb/s fiber links (Case IV) was required to alleviate routing/scheduling bottlenecks and enable $r_{max} = 100$ Mb/s, corresponding to 4G LTE data rates. We note that this numerical optimization result (i.e. 2.5 Gb/s fiber-optic backhaul rate for $n = 20$ cells in a last-mile scenario) is in line with previous analytical and experimental evaluations of 24–25 Gb/s/λ optical MBH rates for $n \approx 200$ cell last-mile backhaul [13]. Moreover, as shown in Fig. 4(b) for Case V, a further upgrade of legacy sites of Fig. 4(a) to 10 Gb/s fiber backhaul provided virtually no r_{max} gains because, in this case, end-to-end throughput was limited by the substantially lower rates on the wireless backhaul links. This was confirmed by the results of Case VI, where r_{max}=141.1 Mb/s was achieved by upgrading legacy MBH sites to 2.5 Gb/s fiber links and by adopting more advanced antenna directionality to increase the point-to-point wireless pre-aggregation segment MBH rates.

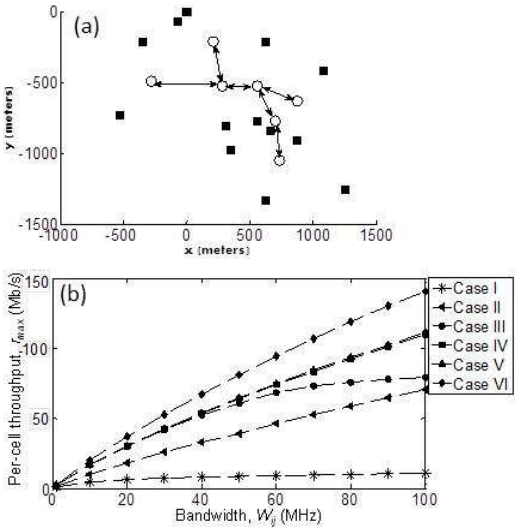

Fig. 4 (a) Legacy macro/new small cell sites map assumption. (b) Per-cell throughput rate, r_{max}, versus bandwidth, W_{ij} (MHz); Case I: pre-aggregation=omni-directional wireless, aggregation =pt-to-pt wireless ($\theta_{ij} = \theta_{ji} = 30°$); Case II: pre-aggregation=pt-to-pt wireless ($\theta_{ij} = \theta_{ji} = 30°$), aggregation=pt-to-pt wireless ($\theta_{ij} = \theta_{ji} = 15°$); Case III: pre-aggregation=pt-to-pt wireless ($\theta_{ij} = \theta_{ji} = 30°$), aggregation=1 Gb/s fiber; Case IV: pre-aggregation=pt-to-pt wireless ($\theta_{ij} = \theta_{ji} = 30°$), aggregation = 2.5 Gb/s fiber; Case V: pre-aggregation=pt-to-pt wireless ($\theta_{ij} = \theta_{ji} = 30°$), aggregation=10 Gb/s fiber; Case VI: pre-aggregation=pt-to-pt wireless ($\theta_{ij} = \theta_{ji} = 15°$), aggregation = 2.5 Gb/s fiber [6].

3. Experimental Demonstration of OFDMA-Based λ Overlay Scenario onto Legacy PON for MBH Application

3.1 Flex-Grid λ-Flow for OFDMA-Based MBH Overlay onto Legacy PON

To deal with continuously changing traffic demands, dynamic service provision overlaying new communication channels on deployed infrastructure can be an attractive solution. Figure 5 shows the software-defined OpenFlow1.0-based flex-grid λ-flow architecture of [5]. 12 Gb/s OFDMA signal for downstream and two 10 Gb/s OOK signals for upstream were overlaid to support new applications, such as MBH over existing PON architectures. In order to minimize negative impact on the live legacy channels due to the new λ overlays, wavelength domain overlap between the newly overlaid and existing signals was avoided by control-

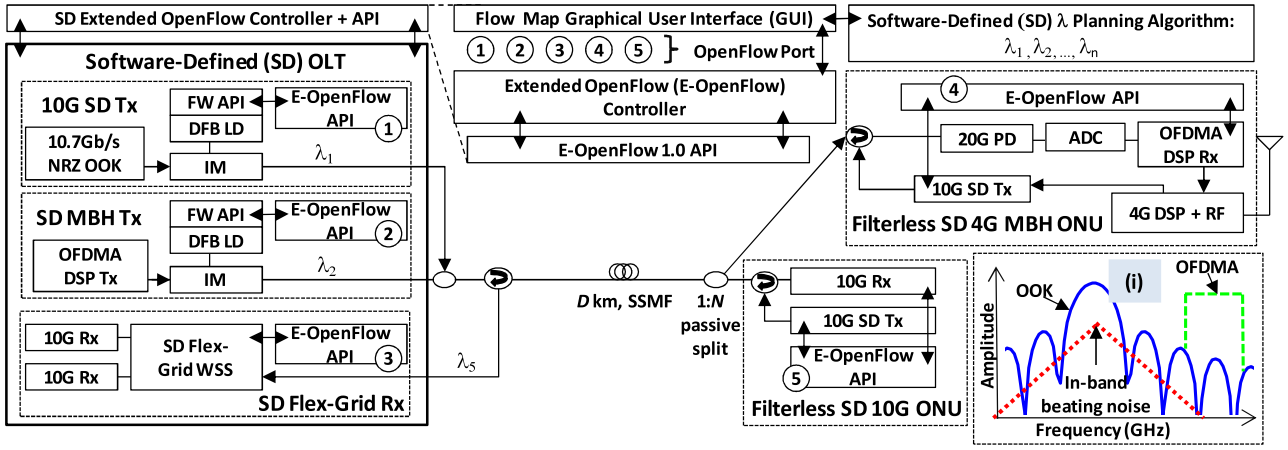

Fig. 5 Flex-Grid λ-Flow architecture for OFDMA-based MBH overlay onto legacy PON. Tx: transmitter; Rx: receiver; FW: firmware; IM: intensity modulator; DFB-LD: distributed feedback laser diode; SSMF: standard single mode fiber; ADC: analog to digital converter; RF: radio frequency.

ling wavelengths of the overlaid signals. Frequency domain overlap also needs to be taken into account for downstream in order to avoid upgrading existing 10G ONUs, because the existing ONUs can receive the overlaid optical signal together with the legacy signal if both pass through an embedded wavelength de-multiplexing filter designed to satisfying legacy wideband wavelength allocation standards. The frequency domain overlap was minimized by setting the newly overlaid OFDMA frequency at a higher sub-λ frequency range, differentiating itself from the existing OOK signal in the electrical spectral domain as shown in an inset figure Fig. 5(i). A flexible grid wavelength selective switch (Flex-Grid WSS) was used to de-multiplex the newly overlaid upstream 10G signals at the relatively cost-tolerant OLT side. Flow management of the overlaid signals and wavelength control were performed by an extended OpenFlow controller via its application interface (API). To admit/control overlaid signals easily, the OpenFlow controller assigns port numbers for each Tx/Rx, and virtualizes physical channels as logical flows.

The performance of this experiment, however, was restricted to 1:64 passive splitting ratio and 20 km of SSMF transmission distance due to signal degradation caused by residual frequency domain overlapping of the OFDMA-based overlaid signal and the legacy 10G OOK signal in the downstream. We can improve transmission performance of either one of these signals by increasing the relative optical power; however, this approach produces further degradation on the other signal. Figure 6(a) shows RF OFDMA signal spectrum measured after direct detection at optical back-to-back (BtB). Main frequency components of the OFDMA signal as a result of its carrier-signal beating fall down around 11–15 GHz, and are automatically cut by a built-in low pass filter (LPF) in general 10G ONUs, as shown in Fig. 6(b), inducing negligible degradation on the legacy 10G OOK signal quality. However, non-negligible OFDMA spectrum components as a result of its signal-signal beating can be seen around 0–4 GHz, and accordingly induce

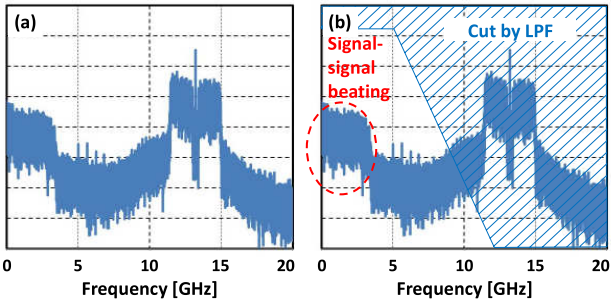

Fig. 6 RF OFDMA signal spectrum measured after direct detection. (a) Raw spectrum; (b) Spectrum with 10G LPF bandwidth

degradation on the legacy 10G OOK signal quality. To mitigate the degradation, we need to create margin for the OFDMA signal, improving its transmission performance, and increase relative optical power of the 10G OOK using the margin. This can be done through optical Nyquist filtering of legacy 10G OOK [7].

3.2 Nyquist Optical Filtering for Legacy 10 Gb/s OOK Signals for OFDMA Signal Quality Improvement

Figure 7(a) plots the baseband 10G OOK spectrum at optical BtB, showing the significant spectral component that exists beyond the main 10G OOK signal lobe. It is this component that creates OFDMA/OOK interference which strongly degrades the OFDMA signal, restricting transmission distance and splitting ratio of [5]. We thus propose to shape the 10G signal spectrum aiming to eliminate the problematic spectral component to improve OFDMA signal performance, while also inducing no signal quality degradation on the 10G signal. The Nyquist pulse-shaping criterion given by Eq. (6) is the key requirement for achieving zero inter-symbol-interference (ISI) in high-speed serial transmission [14].

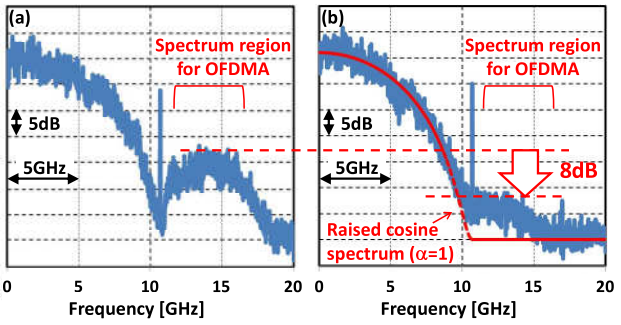

Fig. 7 Baseband 10G OOK spectrum after direct detection for: (a) no optical filtering; (b) after optical Nyquist filtering.

$$\sum_{k=-\infty}^{+\infty} H\left(f-\frac{k}{T}\right)=T. \tag{6}$$

In Eq. (6), k indexes positive and negative integers, T is the symbol time, and H is the Fourier transform of the channel impulse response $h(t)$. In all previously reported Nyquist-shaped optical transmission experiments [15]–[18], advanced multi-level modulation and coherent detection were needed to produce a sharp rectangular spectrum that satisfies Eq. (6) while maximizing wavelength-domain spectral efficiency.

However, such a rectangular spectrum can only be achieved by very sharp optical, electrical or digital filtering that cuts all spectral components beyond the half symbol rate, $1/2T$. In practice, a highly common implementation for rectangular Nyquist shaping is setting the excess bandwidth factor (in other words, the roll-off factor), α, close to zero in the raised cosine spectrum shape $X_{rc}(f)$ given by

$$X_{rc}(f)=\begin{cases} T, & 0\le|f|\le\frac{1-\alpha}{2T} \\ \frac{T}{2}\left[1+\cos\frac{\pi T}{\alpha}\left(|f|-\frac{1-\alpha}{2T}\right)\right], & \frac{1-\alpha}{2T}<|f|\le\frac{1+\alpha}{2T} \\ 0, & \frac{1+\alpha}{2T}<|f| \end{cases}. \tag{7}$$

We observe from Eq. (7) that every value of α satisfying $0 \le \alpha \le 1$ will meet the Nyquist criterion given by Eq. (6), but larger α values will greatly reduce filtering complexity. In this work, we thus present OLT-side $\alpha = 1$ raised cosine optical Nyquist filtering of legacy 10G OOK signals to achieve OFDMA/OOK interference reduction without any ONU-side optics upgrades [7]. We introduce OLT-side Nyquist pulse shaping following Eq. (7) with $\alpha = 1$, and eliminate this problematic OOK spectrum component without introducing ISI and without degrading 10G OOK performance. To confirm this assertion, the optically Nyquist-filtered 10G OOK spectrum was obtained using a programmable optical filter with 1-GHz resolution and a normalized raised cosine spectrum of Eq. (7) with $\alpha = 1$ are shown in Fig. 7(b), confirming a strong match between the two, with about 8 dB suppression of the undesirable OOK spectral component in the radio frequency (RF) OFDMA spectrum region.

Figure 8 plots the measured BER of 10G OOK BtB with and without the proposed optical Nyquist filtering, showing negligible degradation and verifying the zero-ISI

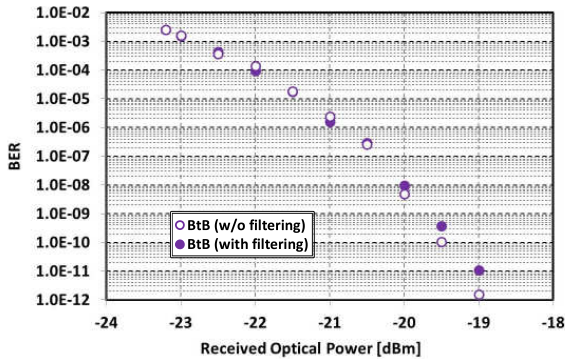

Fig. 8 Measured bit error rate at optical back to back. Hollow circles: no optical filtering; solid circles: optical Nyquist filtering [12].

Nyquist filtering property. A residual OOK spectral component in the 11–15 GHz range in Fig. 7(b) occurs due to the gradual roll-off characteristic of the optical filter used in the experiment, however it can be eliminated by using an optical filter with sharper roll-off characteristic. By eliminating the problematic frequency components of 10G OOK signal without inducing degradation, OFDMA signal performance is expected to be improved resulting in increasing margin, 10G OOK signal performance can also be improved by increasing its relative optical power consuming the created margin.

3.3 Experimental Setup and Results

We experimentally demonstrated OFDMA/OOK interference reduction through the proposed optical Nyquist filtering approach [7]. Figure 9 shows the experimental setup. A commercially available 10.7 Gb/s NRZ-OOK transmitter featuring output wavelength at 1550.92 nm, and a narrowband tunable optical filter (NB-TOF) with 8-GHz bandwidth were used to generate the optical Nyquist filtered 10G OOK signal. A 12.75 Gb/s OFDM signal (3.1875 GHz, 16-QAM symbols, FFT size of 256, 20% FEC and 7.5% training overhead) was generated offline, output continuously by a 12 GS/s arbitrary waveform generator (AWG), and up-converted to f_{RF} = 13.2 GHz. An external cavity laser (ECL) with the wavelength at 1551.32 nm, a 40-GHz optical intensity modulator (IM) and a tunable optical filter (TOF) were used to generate the optical single sideband OFDMA signal. As confirmed in [5], wavelength spacing of 40 GHz resulted in a small amount of degradation in OFDMA signal quality, thus we set the wavelength spacing at 50 GHz in this experiment. The launch powers of the OFDMA and 10G OOK signals were set to 15.0 dBm and 13.0 dBm respectively. The inset figure Fig. 9(i) shows the optical spectrum at the transmitter end, showing a sharpened 10G OOK spectrum due to the NB-TOF, and a single sideband OFDMA signal spectrum with 2 dB higher optical power compared to 10G OOK signal. We should remark here that the optical power difference of these two signals was set smaller than the previous experiment (4 dB) [5], resulting in higher relative 10G OOK optical power and anticipating OFDMA sig-

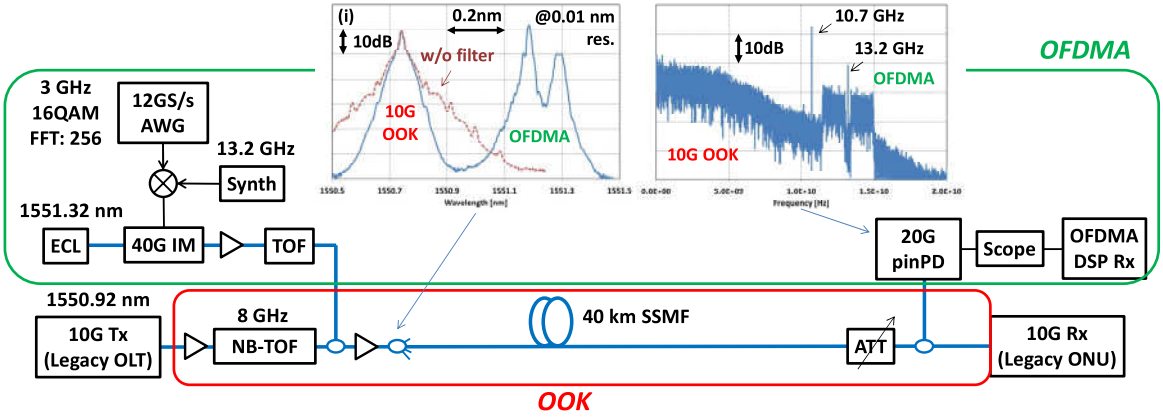

Fig. 9 Experimental setup of joint OFDMA and OOK signal overlay with 40 km SSMF and 1:128 split ratio transmission using optical Nyquist filtering [12]. Synth: synthesizer; TOF: tunable optical filter; NB-TOF: narrow band tunable optical filter.

nal performance improvement thanks to the optical Nyquist filtering of the 10G OOK signal. The total launch power of 17.1 dBm satisfied class 1M requirements for per-fiber launch power [19]. After 40 km standard SSMF, an optical attenuator (ATT) was used to emulate total loss for 1:128 passive split conditions. A 20 GHz pin photodiode (PD) was used to O/E-convert OFDMA signal and a 40 GS/s real-time scope was used to digitize the signal. The OFDMA BER was computed off-line based on 0.25M measured bits. Only digital filtering was used in digital signal processing to remove interference from the 10G OOK signal. The 10G OOK BER was measured using the 7% overhead FEC decoder embedded in a commercial 10G receiver, based on pre-FEC error counts over the period of one minute. Figures 10(a) and (b) show the measured BER for OFDMA and OOK signals, respectively. As shown in Fig. 10(a), when optical Nyquist filtering was not applied on 10G OOK (hollow red squares), the BER of the OFDMA signal after 40-km transmission always exceeded the 20% overhead hard decision (HD) FEC limit of 1.1×10^{-2} [20], [21]. With 10G OOK Nyquist filtering (filled red squares), however, the OFDMA BER was significantly improved to satisfy the FEC limit after 40-km SSMF and 1:128 split (−14.2 dBm received power after 29 dB of total attenuation). Moreover, for −11.2 dBm received power, the OFDMA BER was under 3.8×10^{-3}, revealing that optical Nyquist filtering also enables the reduction of OFDMA FEC overhead from 20% to just 7% (with FEC limit BER is 3.8×10^{-3} [22]) for 40-km SSMF with 1:64 split λ-overlay scenarios. As shown in Fig. 10(b), the 10G OOK signal exhibited no significant performance degradation due to optical Nyquist filtering, with BER remaining under the FEC limit of 3.8×10^{-3} after 40-km SSMF and 1:128 split (−16.2 dBm received power after 29 dB total attenuation). Finally, we could also improve the signal quality of legacy 10G OOK and increase the margin from the previous experimental condition [5] (from green triangles to red squares, Fig. 10(b)). The gain in OOK signal margin is attributed favorable Nyquist filtering effects that enabled the reduction of OFDMA signal power and, consequently, reduced OFDMA-based signal-signal beating (Fig. 6).

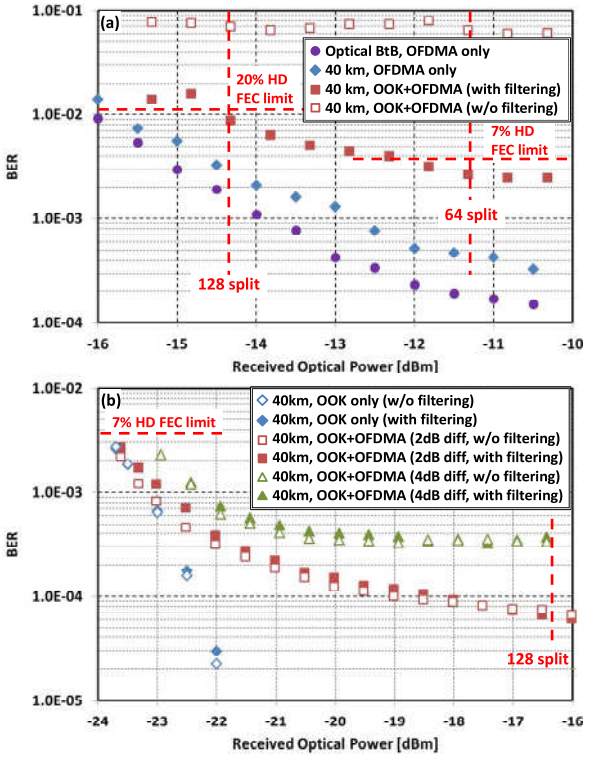

Fig. 10 Measured bit error rates for: (a) OFDMA signal; and (b) 10G OOK signal [7].

4. Conclusion

We have surveyed SDN-based efficient network resource usage for future cost-effective optical MBH networks, focusing on key principles and performance enhancements. We first discussed a centralized SDN-based throughput optimization algorithm for heterogeneous optical/wireless MBH networks. The first OLT-side optical Nyquist filtering of

legacy 10G OOK signals was then proposed and evaluated, enabling dynamic >10 Gb/s OFDMA λ-overlays for MBH over legacy PON with 40-km transmission distances and 1:128 passive splitting ratios, without any ONU-side optics upgrades.

References

[1] J. Kani, F. Bourgart, A. Cui, A. Rafel, M. Campbell, R. Davey, and S. Rodrigues, "Next-generation PON — Part I: Technology roadmap and general requirements," IEEE Commun. Mag., vol.47, no.11, pp.43–49, 2009.
[2] P. Chanclow, A. Cui, F. Geilhardt, H. Nakamura, and D. Nesset, "Network operator requirements for the next generation of optical access networks," IEEE Commun. Mag., vol.26, no.2, pp.8–14, 2012.
[3] N. Yoshimoto, "Operator perspective on next-generation optical access for high-speed mobile backhaul," Proc. OFC/NFOEC 2013, paper Otu2E.1, 2013.
[4] Lightwave, "PON becoming more attractive for mobile backhaul," http://www.lightwaveonline.com/index.html, May 2013.
[5] N. Cvijetic, A. Tanaka, P.N. Ji, S. Murakami, K. Sethuraman, and T. Wang, "First OpenFlow-based software-defined λ-flow architecture for flex-grid OFDMA mobile backhaul over passive optical networks with filterless direct detection ONUs," Proc. OFC/NFOEC 2013, paper PDP5B.2, 2013.
[6] N. Cvijetic and T. Wang, "Software-defined Throughput optimization for next-generation optical mobile backhaul," Proc. OECC 2013, paper TuP1-4, 2013.
[7] A. Tanaka, N. Cvijetic, and T. Wang, "First optical Nyquist filtering of 10 G OOK for OFDMA λ-overlays on 40 km and 1:128 split PON," Proc. OECC 2013, paper PD3-1, 2013.
[8] S. Das, G. Parulkar, and N. McKeown, "Packet and circuit network convergence with OpenFlow," Proc OFC/NFOEC 2010, paper OTuG1, 2010.
[9] N. Cvijetic, "Software-defined optical access networks for multiple broadband access solutions," Proc. OECC 2013, paper TuP2-1, 2013.
[10] K. Kanonakis, N. Cvijetic, I. Tomkos, and T. Wang, "Dynamic software-defined resource optimization in next-generation optical access enabled by OFDMA-based meta-MAC provisioning," J. Lightwave Technol., vol.31, no.14, pp.2296–2306, 2013.
[11] N. Cvijetic, A. Tanaka, K. Kanonakis, and Y.K. Huang, "Software-defined heterogeneous 100 Gb/s mobile backhaul with 1000^{+} per-fiber cell counts," Proc. OECC 2012, paper PDP1-2, 2012.
[12] S. Toumpis and A.J. Goldsmith, "Capacity regions for wireless ad hoc networks," IEEE Trans. Wireless Commun., vol.2, no.4, pp.736–748, 2003.
[13] N. Cvijetic, A. Tanaka, M. Cvijetic, Y.K. Huang, E. Ip, Y. Shao, and T. Wang, "Novel optical access and digital processing architectures for future mobile backhaul," J. Lightwave Technol., vol.31, no.4, pp.621–627, 2013.
[14] J.G. Proakis and M. Salehi, Communication Systems Engineering, Prentice Hall, 2nd ed., 2002.
[15] E. Torrengo, R. Cigliutti, G. Bosco, G. Gavioli, A. Alaimo, A. Carena, V. Curri, F. Forghieri, S. Piciaccia, M. Belmonte, A. Brinciotti, A. La Porta, S. Abrate, and P. Poggiolini, "Transoceanic PM-QPSK terabit superchannel transmission experiments at baud-rate subcarrier spacing," Proc. ECOC 2010, paper We.7.C.2, 2010.
[16] G. Bosco, V. Curri, A. Carena, P. Poggiolini, and F. Forghieri, "On the performance of Nyquist-WDM terabit superchannels based on PM-BPSK, PM-QPSK, PM-8QAM or PM-16QAM subcarriers," J. Lightwave Technol., vol.29, no.1, pp.53–61, 2011.
[17] T.J. Xia, G.A. Wellbrock, A. Tanaka, M.F. Huang, E. Ip, D. Qian, Y.K. Huang, S. Zhang, Y. Zhang, P.N. Ji, Y. Aono, S. Murakami, and T. Tajima, "High capacity field trials of 40.5 Tb/s for LH distance of 1,822 km and 54.2 Tb/s for regional distance of 634 km," Proc. OFC/NFOEC2013, paper PDP5A.4, 2013.
[18] A. Shahpari, J.D. Reis, R. Ferreira, D.M. Neves, M. Lima, and A. Teixeira, "Terabit+ (192 × 10 Gb/s) Nyquist shaped UDWDM coherent PON with upstream and downstream over a 12.8 nm band," Proc. OFC/NFOEC2013, paper PDP5B.3, 2013.
[19] IEC Recommendation 60825-2.
[20] CI-BCH-4^{TM}eFEC, available at www.vitesse.com
[21] B. Li, K.J. Larsen, D. Zibar, and I.T. Monroy, "Over 10 dB net coding gain based on 20% overhead hard decision forward error correction in 100 G optical communication systems," Proc. ECOC2011, paper Tu.6.A.3, 2011.
[22] ITU-T Recommendation G.975.1, Appendix I.9.

Akihiro Tanaka received the B.E. and M.E. degrees in engineering physics and mechanics from Kyoto University, Kyoto, Japan, in 1999 and 2001, respectively. In 2001, he joined NEC Corporation, Kawasaki, Japan, where he was involved in research and development of long-haul, high-capacity optical transmission systems. In 2003, he started research on practical application of quantum key distribution, focusing on high-speed key generation, long-term stable operation, and networking architectures. He is currently with NEC Laboratories America, Princeton, NJ, where he is working on transport SDN architecture for metro/access network. He received the Young Researcher's Award from the Institute of Electronics, Information and Communication Engineers (IEICE), Japan, in 2006.

Neda Cvijetic received the B.S. (summa cum laude), M.S. and Ph.D. degrees in electrical engineering from the University of Virginia, Charlottesville, in 2004, 2005, and 2008, respectively. Since 2008, she has worked as a Research Staff Member in the Broadband and Mobile Networking Department at NEC Laboratories America, Princeton, NJ. She is also currently a member of the adjunct faculty at the Department of Electrical Engineering at Columbia University, as well as an Associate Editor for IEEE Photonics Technology Letters (PTL). Her research interests include advanced modulation, detection and digital signal processing (DSP) for high-speed optical transmission, optical-wireless convergence, and next-generation optical access networks.